

ARTICLE

Tc_n and Tc_n@C₇₀ Endohedral Metalofullerenes: *ab initio* Spin-density-functional Calculations[†]

Li-jing Zeng, Ke Deng*

CAS Key Laboratory of Standardization and Measurement for Nanotechnology, National Center for Nanoscience and Technology (NCNST), Beijing 100190, China

(Dated: Received on July 3, 2015; Accepted on July 14, 2015)

Ab initio spin-density-functional calculations have been performed to study the equilibrium structural, electronic, and magnetic properties of Tc_n and Tc_n@C₇₀ endohedral metalofullerenes. Our results indicate that C₇₀ can encapsulate Tc_n clusters with up to $n=9$ atoms. Except $n=2$, the formation of Tc_n@C₇₀ endohedral metalofullerenes is predicted to be exothermic when $n \leq 5$, while the encapsulation process becomes increasingly endothermic beyond $n=5$. When encapsulating into the C₇₀ cage, the geometries as well as electronic structures of the Tc cluster undergo comparative changes. Especially, compared to the isolated Tc_n clusters, the total magnetic moments of Tc_n@C₇₀ reduce significantly. The analyses of the orbital population, Hirshfeld population and density of states show that electrons transfer from the Tc cluster to the carbon cage through the Tc–C efficient hybridization, which is responsible for such reduction of the whole magnetism.

Key words: Density functional theory, Endohedral metalofullerenes, Tc_n@C₇₀, Vienna *ab initio* simulation package

I. INTRODUCTION

Endohedral metallofullerenes (EMFs), which encapsulate metal atoms inside the fullerene cage, are promising materials in biomedical and material sciences [1]. By changing the nature and composition of the encapsulated species, the EMFs exhibit many novel properties which are quite different from those of the empty fullerenes [2–4]. The unique electrical, magnetic, and optical properties make them attractive for a vast number of nanotechnology applications in the material fields [3]. In particular, owing to their high paramagnetic and radioactive properties, the radionuclide-filled EMFs (Pb@C₆₀, Tb@C₈₂ [5], Gd@C₆₀ [6], Gd@C₈₂ [7]) have been as potentially valuable candidates in biomedical and therapeutic radiopharmaceutical fields [8].

Technetium (Tc), the lowest atomic number element without any stable isotopes, is very expensive and radioactive [9]. Its short-lived gamma ray, ^{99m}Tc, is widely used in nuclear medicine for variously diagnostic tests [10–12]. Its long-lived technetium isotopes are produced in sizable quantities from the nuclear fuel cycle and constitute a crucial issue in the fields of nuclear waste management [13–15].

Although extensive researches have been performed

on the radionuclide-filled EMFs [16, 17], the investigations for the metalofullerenes containing technetium atoms are still scarce. Experimentally, ^{99m}Tc@C₇₀ were firstly produced, characterized and purified by Karam *et al.* in 1997 [18]. Using the ion implantation technique, Cvetičanin *et al.* have studied the endohedral fullerenes of different elements by surface ionization mass spectrometry and observed ionization energy (IE) of ^{99m}Tc@C₇₀ (5.3 eV) [17]. However, recently, Dustebek *et al.* have encapsulated ^{99m}Tc in C₇₀, and reported the measured ionization energy is 9.57 ± 0.25 eV [19]. Obviously, a fully theoretical investigation of structural and electronic properties for Tc_n@C₇₀ isomers is lacking and imperative.

In this work, using the density functional theory (DFT), we carry out a systematic study on the structural, electronic, and magnetic properties of Tc_n@C₇₀ isomers ($n=1-9$). We discuss the dependency of the encapsulation energy on the size of encapsulating Tc_n clusters. We also map out the tendency of the detailed electronic and magnetic properties for the Tc_n clusters and Tc_n@C₇₀ ($n=1-7$) and compare their discrepancy. We analyze the significant reduction of the magnetic moments of Tc_n@C₇₀ respect to the free Tc_n clusters. Our first-principles study should provide useful insights into the research for EMFs.

II. COMPUTATIONAL METHOD

Density functional theory (DFT) calculations have been performed by using the Vienna *ab initio* simu-

[†]Dedicated to Professor Qing-shi Zhu on the occasion of his 70th birthday.

*Author to whom correspondence should be addressed. E-mail: kdeng@nanoctr.cn

lation package (VASP) [20–23]. Spin-polarized general gradient approximation (GGA) [24] of Perdew and Wang (PW91) [25] is implemented in all calculations. Pure functionals such as PW91 generally achieves good performance for transition-metal cluster computations [26, 27], with the accuracy similar to the second-order Moller-Plesset (MP2). The projector augmented wave method (PAW) [22, 28] is used to describe the interaction between valence electrons and ionic cores. The $Tc4p^65s^24d^5$ and $C2s^22p^2$ electrons are treated explicitly as valence electrons in the Kohn-Sham (KS) equations and the remaining cores were represented by PAW pseudopotentials. The KS equations are solved by using Residual minimization method direct inversion in the iterative subspace (RMM-DIIS). The plane wave energy cutoff was set to 500 eV. The calculations are carried out in a large cubic unit cell with size of 15 Å, and we adopt a single k -point (Γ -point) sampling in the Brillouin zone (BZ) integration. Geometries are optimized with symmetry constraints using the conjugate gradient method, accelerated using the Methfessel-Paxton Fermi-level smearing [29] with a Gaussian width of 0.1 eV. Self-consistent field procedure is done with a convergence criterion of 10^{-4} eV on the total energy and 0.01 eV/Å on Hellmann-Feynman forces, respectively.

III. RESULTS AND DISCUSSION

A. Geometries and electronic properties of Tc_n clusters ($n=2-10$)

We have searched all the possible stable isomers for the neutral Tc_n clusters ($n=2-10$), the calculated results are summarized in Fig.1, in which we list the lowest-energy structures, bond lengths, total spin, point-group symmetry, and relative energy for Tc clusters with various sizes.

For Tc_2 , the electronic ground state has a triplet configuration, and the equilibrium bond length is 1.98 Å, which is much shorter than the value of 2.710 Å for Tc metal. This is in line with the recent multiconfiguration second-order perturbation theory prediction of the electronic ground state with a strong quintuple bond ($R_e=1.939$ Å) for Tc_2 [30]. We have examined three triangular geometries (C_{2v} , D_{3h} , C_s symmetries) and linear geometry ($D_{\infty h}$) for Tc_3 . An isosceles triangle (C_{2v} symmetry) with bond lengths of 2.24 and 2.37 Å has been obtained for the ground state of Tc_3 , which is different from the Philippe Weck's result [27]. It is interesting to note that the lowest-energy structure of Tc_4 cluster is still two-dimensional cluster, *i.e.*, a square with D_{4h} symmetry with edges of 2.22 Å in its triplet electronic ground state. This geometry is much more stable (about 0.634 eV) than that of the previously reported ground state of tetrahedron structure (T_d symmetry) [27, 31].

The three-dimensional cluster growth regime starts with Tc_5 . The ground state structure of Tc_5 cluster

is in a distorted pyramidal geometry with bond lengths ranging from 2.22 Å to 2.59 Å, which possesses a quartet multiplicity. It is about 1.31 eV more stable than the trigonal bipyramid structure (bond lengths 2.49, 2.49, 2.57 Å in the base and 2.40, 2.43, 2.43 Å from vertex to base) as shown in Fig.1(d2). A regular octahedral structure (O_h) in the triplet ground state is the energy preferable for Tc_6 , with bond length of 2.43 Å. The less stable geometry is the triangular prism structure (C_{2v}) about 0.56 eV higher.

We predict a new geometry for the Tc_7 cluster, and the optimized structure is distorted truncated prism (C_s). In the quartet multiplicity, this new lowest-lying isomer (Fig.1(f1)) is a noticeable departure from the D_{5h} pentagonal bipyramidal structure reported previously [27], and is about 0.661 eV more stable than the second stable structure.

We have also optimized the structures of Tc_8 , Tc_9 , Tc_{10} , and predicted their new geometries with the lowest and the second lowest-energy in Fig.1, respectively. The new configurations we have obtained are more stable than the previous reported results in Ref.[27]. For Tc_8 , the lowest-energy structure with C_s symmetry is about 0.42 eV more stable than the O_h cubic structure, which is a singlet. For Tc_9 , both the lowest and the second lowest-energy structures have the same C_s symmetry and possess a doublet multiplicity. However, the ground state is distorted pyramid, and energetically preferable about 0.13 eV than the second lowest-energy state. For Tc_{10} , the distorted octagonal bipyramidal structure (C_s) in the triplet is the ground state, which is the energy preferable than the less stable structure about 0.77 eV.

Molecular orbitals analysis can be used as a powerful tool to understand the properties of clusters. We have analyzed the highest occupied molecular orbitals (HOMO) and the lowest occupied molecular orbitals (LUMO) for the lowest-energy structures of Tc_n clusters ($n=2-10$). The orbital populations for the frontier orbitals (HOMO and LUMO) are listed in Table I. To visualize these orbitals, we also show the frontier orbitals in Fig.2. For these structures, the HOMO and LUMO exhibit different spatial characteristics and limited regions of overlap, which leads to an enhanced stability. From Fig.2 and Table I, we can conclude that the HOMO and LUMO of the Tc_n clusters ($n=2-10$) are mainly contributed by $Tc4d$ orbital. For Tc_2 , Fig.2 shows that the frontiers are characteristic of typical 4d orbital. And Table I presents that the non-bonding HOMO and LUMO are 100% based on d_{xy} orbitals. We can notice that when the cluster size increases, some $Tc5s$ orbital and $Tc5p$ orbital contribute to the HOMO and LUMO. In Fig.2, the frontier orbitals of Tc_8 , Tc_9 , and Tc_{10} display more delocalized characters. Combined with the orbital population analyses, it indicates that when the size of the cluster increases, the electron states near the Fermi energy level gradually approach delocalized.

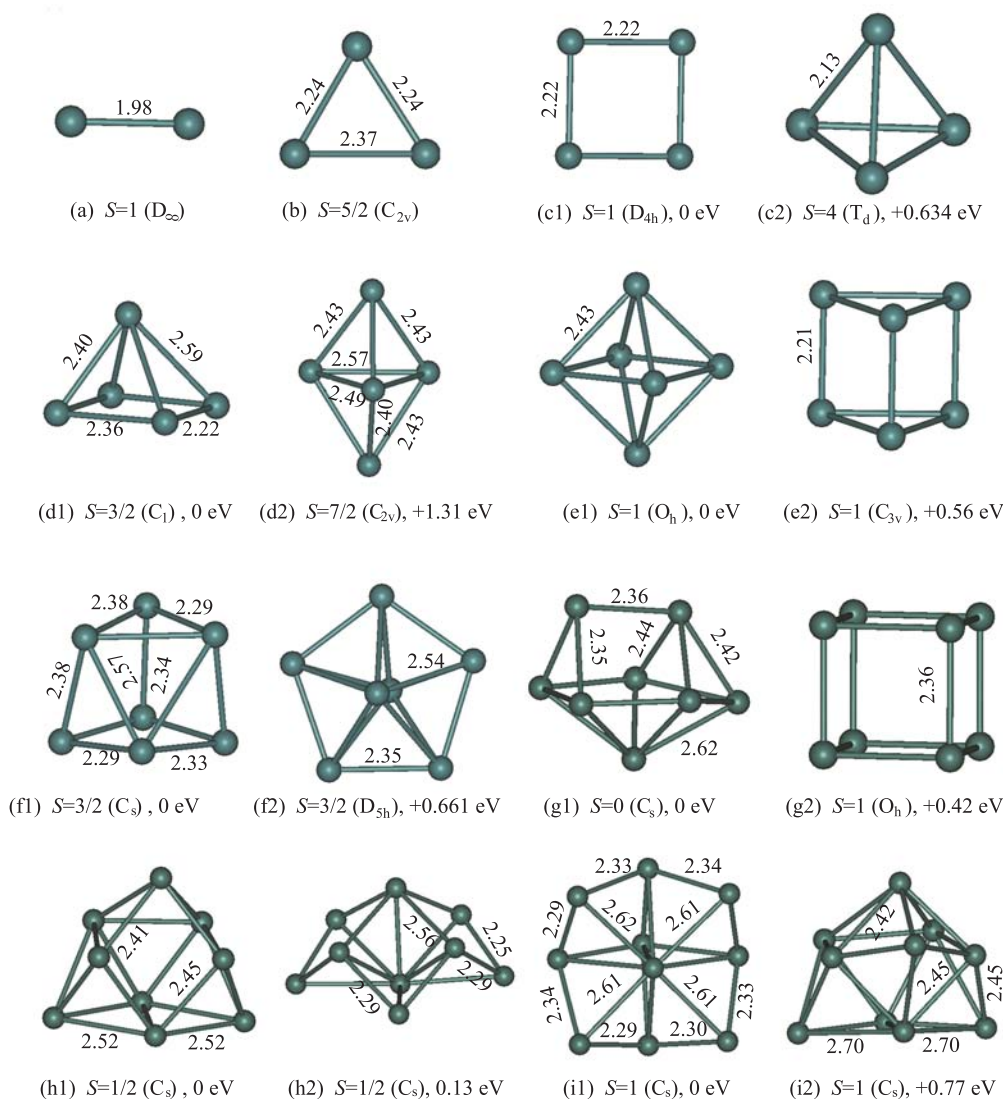


FIG. 1 Optimized low-lying isomers of free Tc_n clusters ($n=2-10$) at the GGA/PW91 level of theory. Additional information listed includes the calculated bond lengths (in Å), total spins (S), point-group symmetry, and relative energy. From Tc₄ to Tc₁₀, both the most stable and the second stable structures are displayed.

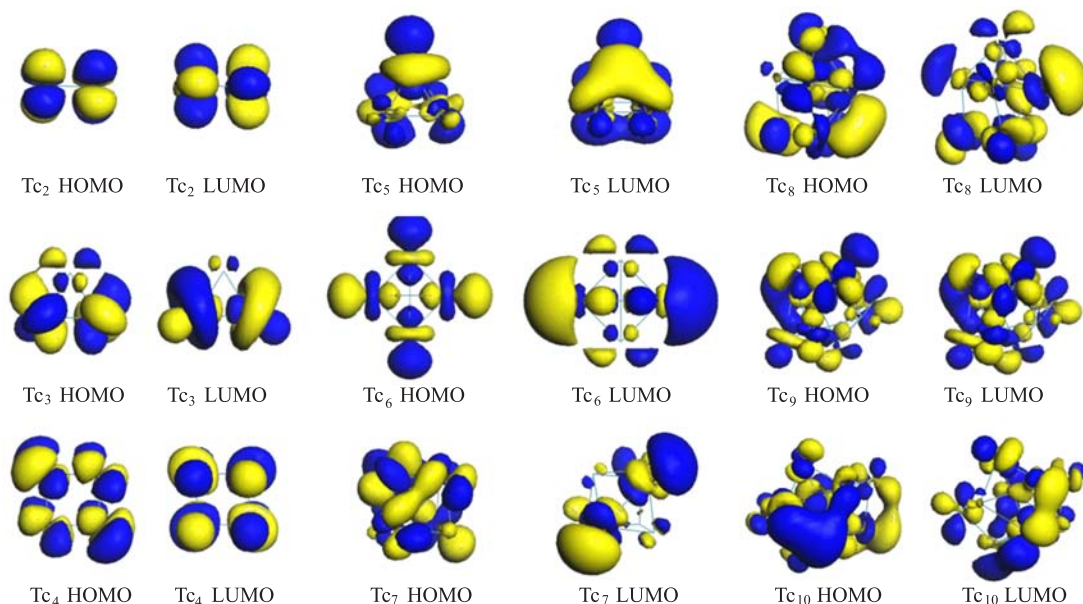
B. Geometries of Tc_n@C₇₀ clusters ($n=1-10$)

The optimized equilibrium structure of the Tc_n@C₇₀ ($n=1-10$) endohedral metallofullerenes are calculated at the GGA/PW91 level of theory. During optimization, we have found that, when Tc₁₀ is encapsulated, the C₇₀ cage becomes collapse. Therefore, we only present the lowest-energy structures of Tc_n@C₇₀ ($n=1-9$) in Fig.3, and investigate the properties of Tc_n@C₇₀ ($n=1-9$).

For a single encapsulated Tc atom, the whole system adopts the C_s symmetry, with Tc atom preferably coordinated to a hexagonal ring of the C₇₀ cage with η^6 hapticities and with the Tc–C bond length of about 2.10 Å. For the Tc₂@C₇₀ EMF, the lowest-energy structure adopts the C₁ symmetry as a whole, with Tc dimer

oriented preferentially along the vertical C₆ symmetry axis of a hexagon in C₇₀ cage. The Tc–C bond length ranges from 2.32 Å to 2.40 Å and the Tc–Tc bond length is measured to be 2.05 Å, slightly longer than that in the isolated dimer (see Fig.1). This is different from the Tc₂@C₆₀ with the Tc–Tc bond length shorter than that in the isolated dimer [32]. Upon encapsulation, the Tc₃ still keeps the C_{2v} point group symmetry, with the Tc–Tc bond lengths in the range from 2.24 Å to 2.37 Å, and the Tc–C bond lengths range of 2.22–2.33 Å.

Tc₄@C₇₀, undergoes the most significant structural transformation, in which Tc₄ cluster transforms from the most stable isolated structure (planar square structure D_{2h}) to the distorted tetrahedron structure. This indicates that the interaction between the Tc cluster

FIG. 2 Calculated HOMO and LUMO for the lowest-energy structures of Tc_n clusters ($n=2-10$).TABLE I Orbital populations for the frontier orbitals of the ground state of Tc_n ($n=2-10$).

	HOMO		LUMO	
	Orbital ^a	Population/%	Orbital ^a	Population/%
Tc ₂	d_{xy}	100	d_{xy}	100
Tc ₃	$d_{yz}/d_{x^2-y^2}/d_{z^2}/s/p$	38/29/29/1/3	$d_{yz}/d_{x^2-y^2}/d_{z^2}/s/p$	4/31/48/8/9
Tc ₄	$d_{x^2-y^2}/p$	90/10	$d_{yz}/d_{z^2}/s$	25/71/4
Tc ₅	$d_{yz}/d_{x^2-y^2}/d_{z^2}/d_{xz}/d_{xy}/s/p$	5/7/35/33/8/1/11	$d_{yz}/d_{x^2-y^2}/d_{z^2}/d_{xz}/d_{xy}/s/p$	19/16/28/10/10/3/14
Tc ₆	$d_{yz}/d_{z^2}/s/p$	18/62/5/15	$d_{yz}/d_{x^2-y^2}/s/p$	8/11/38/43
Tc ₇	$d_{yz}/d_{x^2-y^2}/d_{z^2}/d_{xz}/d_{xy}/s/p$	18/2/5/30/10/18/17	$d_{yz}/d_{z^2}/d_{xz}/d_{xy}/s/p$	20/13/5/10/24/28
Tc ₈	$d_{yz}/d_{x^2-y^2}/d_{z^2}/d_{xz}/d_{xy}/s/p$	28/9/23/14/9/1/16	$d_{yz}/d_{x^2-y^2}/d_{z^2}/d_{xz}/d_{xy}/s/p$	20/2/17/2/8/23/28
Tc ₉	$d_{yz}/d_{x^2-y^2}/d_{z^2}/d_{xz}/d_{xy}/s/p$	15/13/31/9/18/1/13	$d_{yz}/d_{x^2-y^2}/d_{z^2}/d_{xz}/d_{xy}/p$	16/12/33/9/17/13
Tc ₁₀	$d_{yz}/d_{x^2-y^2}/d_{z^2}/d_{xz}/d_{xy}/s/p$	17/8/7/24/12/13/19	$d_{yz}/d_{x^2-y^2}/d_{z^2}/d_{xz}/d_{xy}/s/p$	15/19/24/2/12/13/15

Note: the populations correspond to the different orbitals.

^a d represents 4d orbital, s represents 5s orbital, p represents 5p orbital.

and C_{70} has a great influence on the stable geometry of Tc cluster encapsulated. The similar geometry transition also occurs for Tc₅. For the equilibrium structure of Tc₅@C₇₀, the encapsulated metal cluster possesses a trigonal bipyramid with C_s symmetry, which undergoes a distortion with respect to the free Tc₅ cluster (a distorted tetragonal pyramid).

Upon capsulation, the Tc₆ remains octahedron geometry, while it undergoes a distortion, with symmetry transforming from O_h to C_s . Tc–Tc bond lengths are about 2.63 and 2.54 Å in the encapsulated Tc₆ cluster as a result of the Tc–C hybridization.

Though we predict a new geometry (distorted truncated prism C_s) as the most stable free Tc₇ cluster, we find that the Tc₇ cluster in the equilibrium structure of Tc₇@C₇₀ is the pentagonal bipyramid structure. The

Tc–Tc bond lengths are in range from 2.35 Å to 2.66 Å and the Tc–C bond lengths are from 2.06 Å to 2.34 Å.

When Tc₈ cluster encapsulated into the C₇₀ cage, the Tc₈ structure strongly distorted from C_s symmetry to C_1 symmetry. The Tc–Tc bond lengths are in range from 2.36 Å to 2.56 Å and the Tc–C bond lengths are from 2.08 Å to 2.34 Å. For Tc₉@C₇₀, the encapsulated Tc₉ cluster still keeps C_s symmetry, compared to the free Tc₉ structure. The Tc–Tc bond lengths are in range from 2.39 Å to 2.57 Å and the Tc–C bond lengths are from 2.11 Å to 2.30 Å.

C. Encapsulation energy of Tc_n @C₇₀ clusters ($n=1-9$)

In order to identify the dependence of the encapsulated metallofullerenes on the Tc cluster size, we define

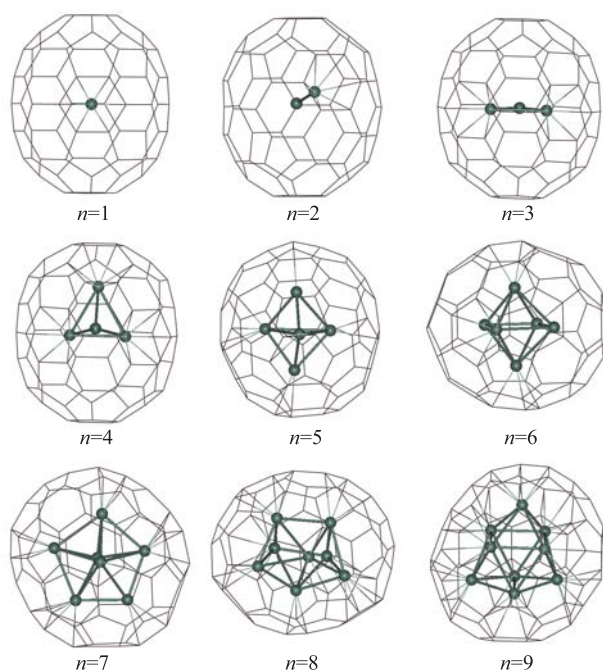


FIG. 3 Optimized equilibrium structures of Tc_n@C₇₀ ($n=1-9$) endohedral metallofullerenes.

the encapsulation energy ΔE_n associated with the reaction $Tc_n + C_{70} \rightarrow Tc_n@C_{70}$ as the following:

$$\Delta E_n = E(Tc_n@C_{70}) - E(Tc_n) - E(C_{70}) \quad (1)$$

where $E(Tc_n@C_{70})$, $E(Tc_n)$, and $E(C_{70})$ are the total free energies at room temperature of the Tc_n@C₇₀, Tc cluster, and C₇₀ cage, respectively. In VASP, the free energy F is defined as $F=H-TS$, where H is the enthalpy, T is the room temperature (298.15 K), and S is entropy. Therefore, ΔE_n can reflect the thermodynamic stability of encapsulated C₇₀. The dependence of the encapsulation energy of the Tc-containing EMFs on the size of the encapsulated Tc cluster is presented in Fig.4.

The encapsulation of a single Tc atom is exothermic, with the capsulation energy $\Delta E=-1.05$ eV. While it is endothermic for Tc dimer to encapsulate into C₇₀ cage, with the positive encapsulation energy $\Delta E=+0.43$ eV. The capsulation energies of Tc₃@C₇₀, Tc₄@C₇₀, and Tc₅@C₇₀ are -0.75 , -1.27 , and -0.20 eV, respectively, which means that the formations of these EMFs are exothermic. These negative encapsulation energies indicate that the creation of Tc-C bonds cause stabilization enhancement of the EMFs. We notice that the encapsulation energy of Tc₄@C₇₀ is the most strongly exothermic. For the encapsulation of Tc₆@C₇₀, Tc₇@C₇₀, and Tc₈@C₇₀, the ΔE are positive ($\Delta E=+3.42$, $+3.52$, and $+7.26$ eV, respectively). Beyond $n>5$, the evolution of the computed encapsulation energy steeply increase positively as a function of the cluster size. Especially, when $n=9$, the encapsulation energy of Tc₉@C₇₀ is $+10.05$ eV. This means the

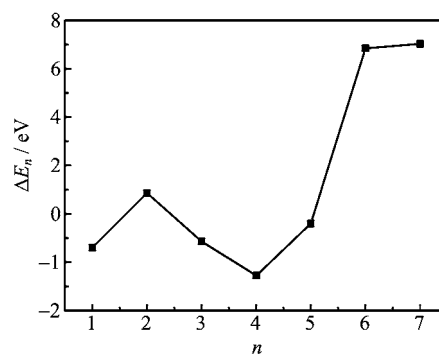


FIG. 4 Dependence of the encapsulation energy ΔE_n , associated with the $Tc_n + C_{70} \rightarrow Tc_n@C_{70}$ reaction, on the cluster size.

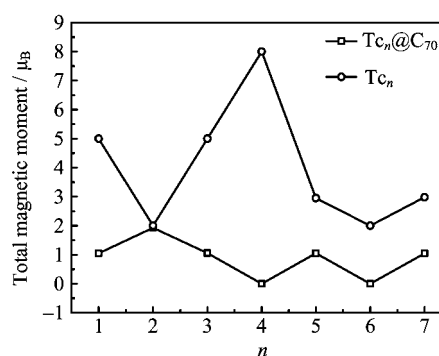


FIG. 5 Dependence of the total electronic magnetic moments in free Tc_n clusters and in Tc_n@C₇₀ endohedral metallofullerenes on the cluster size n .

less probability to produce the corresponding Tc_n@C₇₀ EMFs. Therefore, we only discuss the electronic and magnetic properties of Tc_n@C₇₀ ($n=1-7$) in the following.

D. Electronic and magnetic properties of Tc_n@C₇₀

We have investigated the magnetic properties of the Tc_n and Tc_n@C₇₀ systems, and illustrated the total magnetic moments varying with cluster size n in Fig.5. Though Tc is nonmagnetic as bulk metal [33], the figure shows that the free Tc clusters ($n=1-7$) are with paramagnetic moments, which should be attributed to the unpaired electrons in the highest occupied level in the clusters. Comparing to the isolated Tc_n clusters, with the exception of $n=2$, the total magnetic moments of Tc_n@C₇₀ reduce significantly. Especially, we observe that the calculated magnetic moment of Tc_n@C₇₀ EMFs is zero for $n=4$ and $n=6$. And the magnetic moment of the Tc₂@C₇₀ remains unchanged compared with the isolated Tc₂ cluster.

It is interesting to analyze why the significant reduction occurs for the magnetic moments of the Tc-containing EMFs. Magnetic moments reflect the electron distribution and the bonding character of the sys-

TABLE II Orbital populations for the frontier orbitals of the ground state of $Tc_n@C_{70}$ ($n=1-7$).

	HOMO		LUMO	
	Orbital	Population/%	Orbital	Population/%
$Tc_1@C_{70}$	Tc4d/Tc5p/C2p	25/3/72	Tc4d/Tc5p/C2p	22/2/76
$Tc_2@C_{70}$	Tc4d/C2p	38/62	Tc4d/C2p	12/88
$Tc_3@C_{70}$	Tc4d/Tc5s/Tc5p/C2p	8/43/16/33	Tc4d/Tc5s/Tc5p/C2p	13/7/2/78
$Tc_4@C_{70}$	Tc4d/Tc5s/Tc5p/C2p	15/28/16/41	Tc4d/C2p	65/35
$Tc_5@C_{70}$	Tc4d/C2p	44/56/	Tc4d/Tc5s/Tc5p/C2p	43/2/5/54
$Tc_6@C_{70}$	Tc4d/Tc5s/Tc5p/C2p	47/8/9/36	Tc4d/Tc5s/Tc5p/C2p	29/2/2/67
$Tc_7@C_{70}$	Tc4d/Tc5p/C2p	56/3/41	Tc4d/Tc5p/C2p	57/3/40

Note: the population correspond to the different orbitals.

TABLE III The Hirshfeld charge population for Tc and C atoms in the ground states of $Tc_n@C_{70}$ ($n=1-7$).

	Effective charge/e	
	Tc	C
$Tc_1@C_{70}$	0.246	-0.251
$Tc_2@C_{70}$	0.131	-0.136
$Tc_3@C_{70}$	0.131	-0.135
$Tc_4@C_{70}$	0.095	-0.101
$Tc_5@C_{70}$	0.110	-0.115
$Tc_6@C_{70}$	0.009	-0.013
$Tc_7@C_{70}$	0.128	-0.131

tem. It is obvious that the electrons in the HOMO and LUMO near the Fermi energy level mainly affect the bonding character. Therefore, we firstly investigate the orbital populations for the frontier orbitals of the ground state of $Tc_n@C_{70}$ ($n=1-7$). The results are listed in Table II. For the ground state of $Tc_n@C_{70}$ ($n=1-7$), the HOMOs and LUMOs are composed mainly of d-like orbitals (the Tc4d character ranges from 12% to 65%), p-like orbitals (the C2p character ranges from 33% to 88%), and have slight amounts of Tc5s and Tc5p character. We can conclude that in the $Tc_n@C_{70}$ EMFs, the formation of covalent bonds lies between Tc atoms and C shell atoms, and Tc4d and C2p electrons take part in the covalent bonding.

Furthermore, we have performed the Hirshfeld population analyses. The Hirshfeld charge populations for the Tc and C atoms of the $Tc_n@C_{70}$ ($n=1-7$) are presented in Table III. From the table, we can see that the electronic distribution of $Tc_n@C_{70}$ can be characterized by $Tc_n^{\delta+}@C_{70}^{\delta-}$, and averagely about 0.1 electron is transferred from Tc to C. Combined with the analyses of orbital populations for HOMO and LUMOs, this type of charge transfer proceeds almost from Tc4d to C2p. The charge transfer can reduce the unpaired electrons of Tc_n cluster, which is responsible for the decreasing of the magnetic moment.

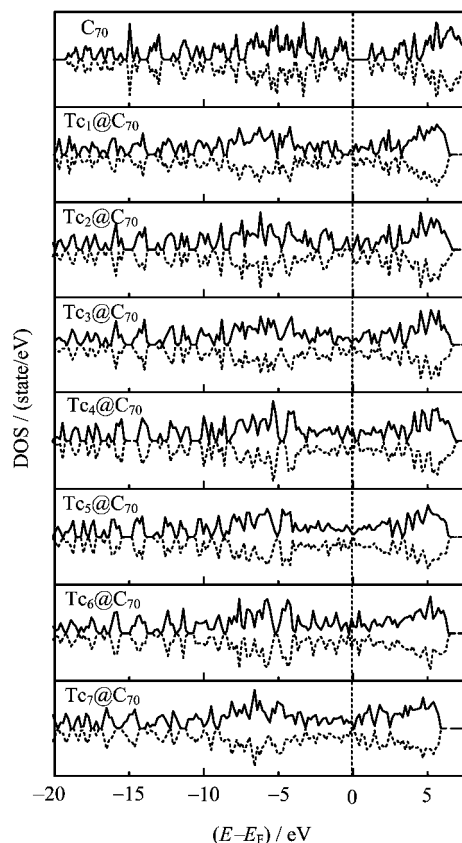


FIG. 6 Total density of states (DOS) of the C_{70} and $Tc_n@C_{70}$ ($n=1-7$). The solid line and dotted line refer to the DOS of electrons of spin-up and spin-down, respectively. The dashed line represents the Fermi energy.

In general, the total density of states (DOS) near to Fermi energy level plays a primary role in determining the magnetism of the system. Thus, the DOS of $Tc_n@C_{70}$ and C_{70} was calculated to understand the above magnetic behaviors, and plotted in Fig.6. In the figure, the isolated C_{70} cage is nonmagnetic, and near the Fermi level, the DOS is zero. This means the magnetism of the EMFs comes from the encapsulation of

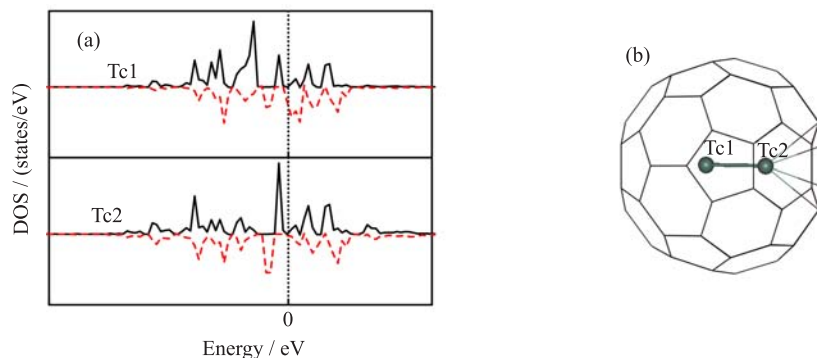


FIG. 7 (a) The 4d orbital density of states of Tc1 atom and Tc2 atom in Tc₂@C₇₀, (b) the geometry of Tc₂@C₇₀.

the Tc clusters.

For Tc₄@C₇₀ and Tc₆@C₇₀, near the Fermi energy level, the DOS of electrons of spin-up and spin-down are totally equal, which indicates that the two systems are nonmagnetic, *i.e.*, the magnetic moment $\mu=0$. While for Tc₁@C₇₀, Tc₂@C₇₀, Tc₃@C₇₀, Tc₅@C₇₀ and Tc₇@C₇₀, the features of the DOS near the Fermi energy level have the characteristic of spin polarization with the magnetic moments.

Especially, we consider why the magnetic moment of Tc₂@C₇₀ is equal to that of the free Tc₂ cluster. In the geometry of Tc₂@C₇₀, in which Tc2 atom coordinates to a hexagonal ring of the C₇₀ cage with η^6 hapticities, and Tc1 atom has no bonding with any C atoms of C₇₀ cage. As mentioned above, encapsulated into the C₇₀ cage, the Tc–Tc bond of Tc₂ lengthens from 1.98 Å to 2.05 Å, which results in the enhancement of the spin polarization of Tc₁ atom near the Fermi energy level (see Fig.7(a)). On the other hand, the formation of covalent bond with the C shell atoms causes the weakening of the spin polarization of Tc₂ atom. Therefore, the magnetic moment of the Tc₂@C₇₀ remains unchanged compared with the isolated Tc₂ cluster.

IV. CONCLUSION

We have investigated the structural, magnetic, and electronic properties of Tc_n and Tc_n@C₇₀ endohedral metalfullerenes using *ab initio* spin-density-functional theory. For the Tc_n cluster, we have proposed some new equilibrium structures of the ground state. The plane structure of Tc₄ is more preferable to the regular tetrahedron structure. And for Tc₇, the anomalous polyhedron structure is the lowest-energy structure, which is different from the previously reported pentagonal bipyramidal structure. We have also predicted new structures for the ground state of Tc₈, Tc₉, and Tc₁₀.

Our results indicate that C₇₀ can encapsulate Tc_n clusters with up to $n=9$ atoms. Except $n=2$, the formation of Tc_n@C₇₀ EMFs is predicted to be exother-

mic when $n \leq 5$, while the encapsulation process becomes increasingly endothermic beyond $n=5$. Upon encapsulation, the geometries as well as electronic structures of the enclosed Tc_n cluster undergo comparatively changes. The analyses of orbital populations show that the HOMO and LUMO of the Tc_n clusters ($n=2-10$) are mainly contributed by Tc4d orbital. Compared to the isolated Tc_n clusters, the total magnetic moments of Tc_n@C₇₀ reduce significantly except Tc₂@C₇₀ in which the magnetic moment maintains its net magnetic moment upon encapsulation. The analyses of orbital populations, Hirshfeld charge populations, and density of states of Tc_n and Tc_n@C₇₀ EMFs show that the magnetic moments of Tc_n@C₇₀ EMFs are mainly due to the spin polarization of Tc4d electrons and C2p electrons. Furthermore, electrons transfer from the Tc cluster to the carbon cage through the Tc–C efficient hybridization, which is responsible for such reduction of the whole magnetism.

V. ACKNOWLEDGMENTS

This work was supported by the National Key Basic Research Program of China (No.2012CB933001), the Chinese Academy of Sciences (No.YZ201318). The CAS Key Laboratory of Standardization and Measurement for Nanotechnology of Chinese Academy of Sciences is acknowledged for computational facilities.

- [1] C. H. Huang, *Rare Earth Coordination Chemistry: Fundamentals and Applications*, John Wiley & Sons, (2010).
- [2] M. Hoinkis, C. S. Yannoni, D. S. Bethune, J. R. Salem, R. D. Johnson, M. S. Crowder, and M. S. de Vries, *Chem. Phys. Lett.* **198**, 461 (1992).
- [3] T. Suzuki, Y. Maruyama, and T. Kato, *Synth. Met.* **70**, 1443 (1995).
- [4] I. E. Kareev, S. F. Lebedkin, V. P. Bubnov, E. B. Yagubskii, I. N. Ioffe, P. A. Khavrel, I. V. Kuvychko,

- S. H. Strauss, and O. V. Boltalina, *Angew. Chem.* **117**, 1880 (2005).
- [5] K. Iwasaki, N. Wanita, S. Hino, D. Yoshimura, T. Okazaki, and H. Shinohara, *Chem. Phys. Lett.* **398**, 389 (2004).
- [6] J. Lu, W. N. Mei, Y. Gao, X. C. Zeng, M. W. Jing, G. P. Li, R. Sabirianov, Z. X. Gao, L. P. You, J. Xu, D. P. Yu, and H. Q. Ye, *Chem. Phys. Lett.* **425**, 82 (2006).
- [7] H. Funasaka, K. Sakurai, Y. Oda, K. Yamamoto, and T. Takahashi, *Chem. Phys. Lett.* **232**, 273 (1995).
- [8] J. Meng, D. L. Wang, P. C. Wang, L. Jia, C. Y. Chen, and X. J. Liang, *J. Nanosci. Nanotechnol.* **10**, 8610 (2010).
- [9] U. Abram and R. Alberto, *J. Brazilian Chem. Soc.* **17**, 1486 (2006).
- [10] P. R. Talbot, J. J. Lloyd, J. S. Snowdena, D. Nearya, and H. J. Testa, *J. Ne. Ne. Psy.* **64**, 306 (1998).
- [11] N. J. Dougall, S. Bruggink, and K. P. Ebmeier, *Am. J. Ger. Ps.* **12**, 554 (2004).
- [12] T. J. Selman, D. M. Luesley, N. Acheson, K. S. Khan, and C. H. Mann, *Gynecologic Oncology* **99**, 206 (2005).
- [13] S. El-Wear, K. German, and V. Peretrukhin, *J. Radioanal. Nucl. Chem.* **157**, 3 (1992).
- [14] K. H. Lieser, *Radiochimica Acta* **63**, 5 (1993).
- [15] N. N. Popova, I. G. Tananaev, S. I. Rovnyi, and B. F. Myasoedov, *Russ. Chem. Rev.* **72**, 101 (2003).
- [16] H. Shinohara, *Rep. Prog. Phys.* **63**, 843 (2000).
- [17] J. Cveticanin, J. Cveticanin, J. Djustebek, M. Veljković, S. Veličković, V. Djordjević, and O. Nešković, *J. Optoelectronics Adv. Mater.* **8**, 1892 (2006).
- [18] L. R. Karam, M. G. Mitch, and B. M. Coursey, *Appl. Radiat. Isot.* **48**, 771 (1997).
- [19] J. B. Đustebek, V. R. Đorđević, J. M. Cveticanin, S.R. Veličković, M. V. Veljković, O. M. Nešković, Z. L. Rakočević, and N. M. Bibić, *Nucl. Instrum. Methods Phys. Res., Sect. B* **268**, 466 (2010).
- [20] G. Kresse and J. Hafner, *Phys. Rev. B* **47**, 558 (1993).
- [21] G. Kresse and J. Hafner, *Phys. Rev. B* **48**, 13115 (1993).
- [22] G. Kresse and D. Joubert, *Phys. Rev. B* **59**, 1758 (1999).
- [23] G. Kresse and J. Hafner, *Phys. Rev. B* **49**, 14251 (1994).
- [24] J. P. Perdew, J. A. Chevary, S. H. Vosko, K. A. Jackson, M. R. Pederson, D. J. Singh, and C. Fiolhais, *Phys. Rev. B* **46**, 6671 (1992).
- [25] J. P. Perdew, K. Burke, and M. Ernzerhof, *Phys. Rev. Lett.* **77**, 3865 (1996).
- [26] F. Poineau, L. Gagliardi, P. M. Forster, A. P. Sattelberger, and K. R. Czerwinski, *Dalton Trans.* **30**, 5954 (2009).
- [27] P. F. Weck, E. Kim, F. Poineau, and K. R. Czerwinski, *Phys. Chem. Chem. Phys.* **11**, 10003 (2009).
- [28] P. E. Blöchl, *Phys. Rev. B* **50**, 17953 (1994).
- [29] M. Methfessel and A. T. Paxton, *Phys. Rev. B* **40**, 3616 (1989).
- [30] A. C. Borin, J. P. Gobbo, and B. O. Roos, *Molecular Phys.* **107**, 1035 (2009).
- [31] R. Sekine, R. Kondo, T. Yamamoto, and J. Onoe, *Radiochemistry* **45**, 233 (2003).
- [32] P. F. Weck, E. Kim, K. R. Czerwinski, and D. Tománek, *Phys. Rev. B* **81**, 125448 (2010).
- [33] V. Moruzzi and P. Marcus, *Phys. Rev. B* **48**, 7665 (1993).